Unsteady Transonic Flow over Wings Including Inviscid/Viscous Interaction

D. P. Rizzetta* and C. J. Borland†
Boeing Military Airplane Company, Seattle, Washington

A numerical procedure is presented for computing the unsteady transonic flowfield about swept wings undergoing time-dependent motions. The outer inviscid portion of the flow is assumed to be governed by the modified unsteady transonic small disturbance potential equation which is integrated in the time domain by means of an alternating direction implicit algorithm. Dominant effects of the shock/boundary-layer interaction are accounted for by a simple empirically defined model. Viscous flow regions adjacent to the wing surface and in the trailing wake are described by a set of integral equations appropriate for compressible turbulent shear layers. The two-dimensional boundary-layer equations are applied quasistatically stripwise across the span. Coupling with the outer inviscid flow is implemented through use of the displacement thickness concept. Validity of the assumptions underlying the method is established by comparison with experimental data for the flow about a high aspect ratio transport wing having an advanced airfoil section.

Nomenclature

a = $(E/c) + 2G_S\xi_y\phi_\eta$
A = $\epsilon M_\infty^2 k^2$
AR = aspect ratio
b = $(F/c^2) + G_S\xi_y^2$
B = $2M_\infty^2 k$
c = local section chord nondimensionalized by c_r (c_s/c_r)
c_r = reference chord
c_s = local section chord
C_E = entrainment coefficient, $\frac{1}{\rho_e U_e}\frac{\mathrm{d}}{\mathrm{d}S}\int_0^\delta \rho U \mathrm{d}N$
C_l = total wing lift coefficient, $2\int_0^{\eta_{\text{tip}}}\int_0^1 (C_p^- - C_p^+)\,\mathrm{d}\xi\mathrm{d}\eta$
C_m = total wing moment coefficient, moment taken about leading edge of root section
C_p = local section pressure coefficient
D_ξ, D_η = type-dependent finite difference operators
E = $1 - M_\infty^2$
f = local instantaneous surface section definition [$z = f(x,t)$]
f_{R_ξ} = local viscous ramp surface slope modification
F = $-\frac{1}{2}(\gamma+1)M_\infty^2$
F_1 = see Eq. (20)
F_2 = see Eq. (21)
g = initial ϕ distribution, $\phi(\xi,\eta,\zeta,0)$
G = $\frac{1}{2}(\gamma-3)M_\infty^2$
G_S = $1 - M_\infty^2$
G_N = $\frac{1}{2}(\gamma-1)M_\infty^2 - 1$
h = initial ϕ_t distribution, $\phi_t(\xi,\eta,\zeta,0)$
H = $-(\gamma-1)M_\infty^2$
H_0 = shape factor, δ^*/θ
$\bar{H}$ = shape parameter, $\frac{1}{\theta}\int_0^\infty \frac{\rho}{\rho_e}\left(1 - \frac{U}{U_e}\right)\mathrm{d}N$
k = reduced frequency, $\omega c_r/U_\infty$
M = Mach number
N = physical normal boundary-layer coordinate
Re_∞ = freestream Reynolds number based upon chord, $\rho_\infty U_\infty c_r/\mu_\infty$
S = physical streamwise boundary-layer coordinate
t = physical time nondimensionalized by $1/\omega$
U = streamwise velocity component
x = physical streamwise coordinate nondimensionalized by c_r
X = $G_N(\xi_y\phi_\xi + \phi_\eta)^2 + H\xi_y\phi_\xi(\xi_y\phi_\xi + \phi_\eta) + c\xi_y(\xi_y\phi_\xi + \phi_\eta)$
y = physical spanwise coordinate nondimensionalized by c_r
Y = $H\phi_\xi(\xi_y\phi_\xi + \phi_\eta) + c\xi_y\phi_\xi$
z = physical normal coordinate nondimensionalized by c_r
α = angle of attack
β = viscous ramp wedge angle
γ = specific heat ratio
δ = boundary-layer thickness
δ^* = displacement thickness, $\int_0^\infty \left(1 - \frac{\rho U}{\rho_e U_e}\right)\mathrm{d}N$
$\delta_\xi, \delta_\eta, \delta_{\zeta\zeta}$ = finite difference operators
$\Delta\xi, \Delta\eta, \Delta\zeta, \Delta t$ = finite difference numerical mesh step sizes
ϵ = 0 for low-frequency approximation; 1 otherwise
ζ = nondimensional transformed normal coordinate
η = nondimensional transformed spanwise coordinate
θ = momentum defect thickness, $\int_0^\infty \frac{\rho U}{\rho_e U_e}\left(1 - \frac{U}{U_e}\right)\mathrm{d}N$
Λ_{LE} = leading-edge sweep angle
Λ_s = local section sweep angle
λ = taper ratio
μ = viscosity coefficient
ξ = nondimensional transformed streamwise coordinate
ξ_o = offset of viscous ramp leading edge from sonic point
ξ_p = length of viscous ramp precursor
ξ_R = length of viscous ramp main body
ξ_s = sonic point location

Presented as Paper 82-0352 at the AIAA 20th Aerospace Sciences Meeting, Orlando, Fla., Jan. 11-14, 1982; submitted Jan. 22, 1982; revision received June 2, 1982.

*Senior Specialist Engineer; presently, Aerospace Engineer, Air Force Wright Aeronautical Laboratories, Wright-Patterson Air Force Base, Ohio. Member AIAA.
†Principal Engineer. Associate Fellow AIAA.

ρ = density
ϕ = perturbation velocity potential function nondimensionalized by $c_r U_\infty$
Φ = physical velocity potential function, $c_r U_\infty (x+\phi)$
ω = circular oscillation frequency

Superscripts

$(\ )^+$ = upper surface
$(\ )^-$ = lower surface
$(\bar{\ })$ = backward difference
$(\tilde{\ })$ = first intermediate solution (prediction)
$(\tilde{\tilde{\ }})$ = second intermediate solution (first correction)
$(\ )^*$ = critical value
n = previous time level
$n+1$ = final solution at new time level (second correction)

Subscripts

e = boundary-layer edge
I,J,K = ξ,η,ζ grid indices
K_p = ζ plane lying above wing surface
K_m = ζ plane lying below wing surface
LE = leading edge
min = minimum
tip = wing tip
t = time derivative
US = upstream
x,y,z; ξ,η,ζ = spatial derivative
2D = two dimensional
3D = three dimensional
∞ = freestream

I. Introduction

SOLUTIONS of steady inviscid transonic flowfields about wings of arbitrary planform are commonly obtained by numerical solution of the differential equation governing the velocity potential function. While this approach necessarily implies that any embedded shock waves are sufficiently weak that rotationality effects may be neglected, it has proven extremely useful for many applications.[1-7] In the case of unsteady flows, few methods capable of generating time accurate three-dimensional flowfields are available currently.[8-12] If the wing may be considered thin, the problem is rendered more tractable by applying the small disturbance assumption. This not only simplifies the governing equation, but also facilitates application of the surface boundary condition.

Time integration of the modified unsteady transonic small disturbance potential equation has proven to be particularly useful. It permits the treatment of nonlinear unsteady three-dimensional flow phenomena including irregular shock wave motion. In addition, the flowfield equation may be coupled directly with the structural equations of motion for an elastic wing which simultaneously are integrated in time in order to obtain a nonlinear aeroelastic solution.[13]

Although unsteady inviscid flowfield solutions can provide a reasonable physical description for a wide variety of flow conditions, they will not be adequate when viscous effects are significant. This is true typically for flows about wings having advanced airfoil sections which involve complex flow structures characterized by the following phenomena: 1) shock/boundary-layer interaction altering the shock strength and location, 2) effective camber modification due to differences in the boundary-layer displacement on the upper and lower wing surfaces, and 3) displacement and camber effects of the near wake. A detailed description of these effects can be provided only through the use of additional equations governing the flow. Numerical solution of the more exact equations appropriate to three-dimensional viscous flows is burdensome in terms of computing resources. For the study of aeroelastic behavior and nonlinear flutter, it is reasonable to perform a more simplified analysis. It is the intent here to account for the gross dominant effects of inviscid/viscous interaction for such applications without degrading the basic efficiency of the inviscid computation. Thus, no attempt will be made to resolve exact details of viscous regions, but rather the effects of viscosity upon the unsteady surface pressure distribution will be determined in order to provide appropriate aerodynamic forces for structural applications.

It is assumed that viscous effects are confined to thin regions immediately adjacent to the wing surface and along the trailing wake. These are then postulated to be in instantaneous equilibrium with the unsteady outer inviscid flow. A simple order of magnitude analysis indicates that this assumption is valid if the reduced frequency of the unsteady wing surface motion is small.[14] As a consequence, a steady form of the equations governing the viscous regions may be applied in a quasisteady fashion. In addition, the viscous equations appropriate for two-dimensional flows will be applied stripwise along the span. For this calculation, however, the streamwise direction is taken as that either normal to the mean of the leading- and trailing-edge sweep angles for locally subsonic strips, or normal to the shock surface for strips where shock waves are present. Thus, the treatment of the viscous equations embodies the concept of simple sweep theory.

The use of two-dimensional boundary-layer equations greatly reduces the amount of computational effort involved in treating viscous regions. Even with an integral formulation, a three-dimensional viscous analysis requires solution of a system of partial differential equations, which can be costly. This is no small consideration for performing aeroelastic analysis which may require a large number of solutions to establish flutter boundaries.

Viscous regions are assumed to be governed by a set of boundary-layer equations appropriate for turbulent flows. For this purpose an integral form of "lag entrainment equations" are employed, which have been used with success for the prediction of turbulent shear layers.[15-17] Coupling with the outer inviscid flow is provided by the displacement thickness concept within the framework of small disturbance theory. The impact of viscous effects upon the potential equation is manifested solely in a modification of the surface and wake boundary conditions. This procedure has proven adequate for a number of both steady and unsteady computations of flows about airfoils.[18-20]

The most complex aspect of viscous transonic flows over wings is that of the shock/boundary-layer interaction. This effect is difficult to represent and resolve correctly for turbulent flows, and troublesome to couple in a numerically stable fashion with the outer inviscid solution. In the case of steady flows, procedures have been developed which achieve this coupling. Such methods commonly involve the use of under-relaxation in an iterative process such that a matching of the two solutions is attained at convergence. Both the physical and numerical difficulties are considerably more involved in the unsteady case. Here, the shock strength and location vary in time as the shock traverses the wing surface. In addition, time accuracy as well as stability is essential.

Much of this difficulty is removed by employing a simple computational artifice to model the displacement effect of the shock/boundary-layer interaction which is used in conjunction with the boundary-layer solution. This is accomplished by augmenting the wing surface geometry with a wedge-nosed ramp that is inserted near the base of the shock in the inviscid calculation. The ramp converts the normal shock to an oblique shock, thereby decreasing its strength, displaces it upstream from its inviscid location, and is free to traverse the wing surface in correspondence with the unsteady shock motion. The magnitude of the ramp angle is allowed to adjust instantaneously to the shock strength and is chosen such that an empirically defined post-shock pressure is

recovered. Application of this ramp model has proven quite useful in both two- and three-dimensional steady computations[21] and more recently in two-dimensional unsteady solutions.[14,22]

II. Unsteady Potential Equation

The equation governing the outer inviscid flow is the modified three-dimensional unsteady transonic small disturbance potential equation which includes higher order terms to ensure proper swept shock jump conditions, and may be written as

$$\frac{\partial}{\partial t}(A\phi_t + B\phi_x) = \frac{\partial}{\partial_x}(E\phi_x + F\phi_x^2 + G\phi_y^2) + \frac{\partial}{\partial y}(\phi_y + H\phi_x\phi_y) + \frac{\partial}{\partial z}(\phi_z) \tag{1}$$

The following shearing transformation is applied in order to map the swept tapered wing planform in the physical domain into a rectangle in the Cartesian computational domain.

$$\xi = \frac{x - x_{LE}(y)}{c(y)}, \qquad \eta = y, \qquad \zeta = z \tag{2}$$

Outboard of the wing tip, a smooth transition to a constant chord section swept at the average of the leading- and trailing-edge sweep angles is applied. In addition, the coefficient G is split into two components, G_S and G_N, such that the streamwise and normal contributions to the spatial differencing of the governing equation may be identified. This decomposition will be useful in the formulation of the numerical solution algorithm. Upon defining a, b, X, and Y, Eq. (1) becomes

$$cA\phi_{tt} + B\phi_{\xi t} = \frac{\partial}{\partial \xi}(a\phi_\xi + b\phi_\xi^2) + 2G_S\phi_\eta\phi_{\xi\eta} + \frac{\partial}{\partial \eta}(c\phi_\eta) + c\frac{\partial^2\phi}{\partial \zeta^2} + \frac{\partial X}{\partial \xi} + \frac{\partial Y}{\partial \eta} \tag{3}$$

It is noted that

$$\frac{\partial}{\partial \xi}(a\phi_\xi + b\phi_\xi^2) + 2G_S\phi_\eta\phi_{\xi\eta} \tag{4}$$

represents the streamwise contribution to the governing equation with the remaining terms on the right-hand side of Eq. (3) comprising the normal portion.

A formal definition of the inviscid problem is completed by prescription of the boundary and initial conditions

far upstream

$$\phi = 0 \tag{5a}$$

far downstream

$$(1/c)\phi_\xi + \epsilon k\phi_t = 0 \tag{5b}$$

wing root

$$\xi_y\phi_\xi + \phi_\eta = 0 \tag{5c}$$

far spanwise

$$\phi_\eta = 0 \tag{5d}$$

far above and below

$$\phi_\zeta = 0 \tag{5e}$$

On the wing surface, the linearized unsteady boundary condition

$$\phi_\zeta^\pm = (1/c)f_\xi^\pm + \epsilon k f_t^\pm \tag{6}$$

is applied on $\zeta = 0^\pm$ for $0 \le \xi \le 1$, $0 \le \eta \le \eta_{tip}$.

Along the trailing vortex sheet in the wake, the following contact conditions are invoked.

$$[(1/c)\phi_\xi + \epsilon k\phi_t] = 0 \tag{7a}$$

$$[\phi_\zeta] = 0 \tag{7b}$$

on $\zeta = 0$ for $\xi > 1$, $0 \le \eta \le \eta_{tip}$, where brackets denote the jump in the enclosed quantity from above to below the vortex sheet.

Finally, the initial conditions

$$\phi(\xi,\eta,\zeta,0) = g(\xi,\eta,\zeta), \quad \phi_t(\xi,\eta,\zeta,0) = h(\xi,\eta,\zeta) \tag{8}$$

are specified.

Once the solution to Eq. (3) is obtained, the local instantaneous pressure coefficient may be determined from the following expression.

$$C_p = -(2/c)\phi_\xi - 2\epsilon k\phi_t \tag{9}$$

III. Viscous Equations

Solution of the equations governing viscous flow regions is predicated upon the quasisteady assumption. Therefore, it is necessary to consider only the steady form of the equations involved in order to extend the flowfield solution from time level t^n to time level $t^{n+1} = t^n + \Delta t$ during the unsteady solution process. In order to evaluate viscous parameters at the new time level, t^{n+1}, all inviscid quantities are obtained from the potential solution at time level t^n. The two-dimensional form of the viscous equations is employed stripwise along the span. However, the streamwise direction is taken as that normal to the local sweep angle Λ_s. The value of Λ_s is equal to that of the incident shock surface for locally supersonic strips or the mean of the leading- and trailing-edge sweep angles for locally subsonic strips.

Viscous Ramp

The viscous ramp model, which is used to simulate the displacement effect of the shock/boundary-layer interaction, is based upon the observation in many steady experimental measurements that the post-shock pressure level for turbulent flow over an airfoil corresponds approximately to that of the oblique shock produced by flow over a compression ramp with a wedge angle equal to that of the detachment angle for the given upstream Mach number. Geometry of the model is depicted schematically in Fig. 1. It consists of a short precursor over which the ramp slope varies linearly from zero to the given wedge angle followed by the main ramp body along which the slope varies quadratically. At the ramp leading edge the ramp height and slope are continuous, and at the downstream end the slope and curvature vanish. The ramp is positioned with respect to the local instantaneous sonic point location and affinely scaled with the shock strength as determined by local conditions upstream of the shock. By offsetting the ramp leading edge a distance ξ_o ahead of the sonic location, the ramp is able to more fully influence the numerical shock profile. The leading edge of the ramp is preceded by a precursor of length ξ_p which has been used in previous unsteady calculations[14,20,22] to moderate passage of the sharp leading edge across computational mesh points,

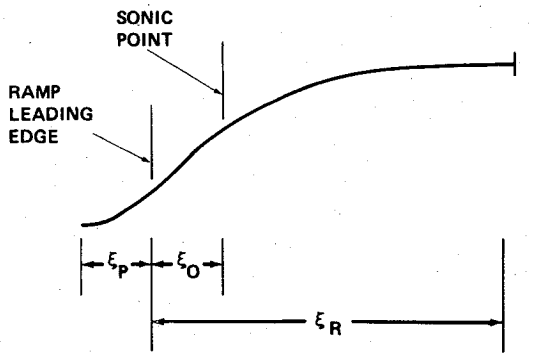

Fig. 1 Viscous ramp geometry.

thereby precluding spurious numerical instabilities. The main body of the ramp has a length of ξ_R where the parameters ξ_p, ξ_o, and ξ_R may be selected for each specific application.

The wedge angle β is obtained directly from the steady two-dimensional form of Eq. (3). A complete derivation may be found in Ref. 20. In addition, the concepts of simple sweep theory are applied to obtain

$$\beta=\left(\frac{2}{F}\right)\left[\frac{-2\cos^2\Lambda_s\,(F/c)\,\phi_{\xi_{US}}-E}{3}\right]^{3/2} \tag{10}$$

where $\phi_{\xi_{US}}$ is evaluated just upstream of the shock. Given $\phi_{\xi_{US}}$ and the sonic point location ξ_s, the ramp slope variation f_{R_ξ} is algebraically defined in terms of ξ, ξ_p, ξ_s, ξ_o, and ξ_R.

Lag Entrainment Equations

The form of the integral boundary-layer equations which will be considered here is that of the lag entrainment equations due to Green.[15] They are predicated upon the boundary-layer assumption that the normal extent of viscous region is small compared to the wing or wake thickness, which necessarily applies to flows at high Reynolds numbers. By integrating the governing partial differential equations in the normal direction and suitably modeling the requisite relationships among the dependent variables, a system of three first-order ordinary differential equations is obtained. Two of the equations result directly from continuity and momentum. The third evolves from the Bradshaw et al.[23] turbulent energy equation, but is formulated in terms of the entrainment concept originally proposed by Head.[24] This yields a streamwise rate equation governing the degree to which the outer inviscid flow merges with the turbulent shear layer.

The lag entrainment equations are briefly summarized here, where the simple sweep concept has been employed for coupling with the inviscid solution. We first define

displacement thickness

$$\delta^*=\int_0^\infty\left(1-\frac{\rho U}{\rho_e U_e}\right)\mathrm{d}N \tag{11}$$

momentum defect thickness

$$\theta=\int_0^\infty\frac{\rho U}{\rho_e U_e}\left(1-\frac{U}{U_e}\right)\mathrm{d}N \tag{12}$$

shape factor

$$H_0=\delta^*/\theta \tag{13}$$

shape parameter

$$\bar{H}=\frac{1}{\theta}\int_0^\infty\frac{\rho}{\rho_e}\left(1-\frac{U}{U_e}\right)\mathrm{d}N \tag{14}$$

entrainment coefficient

$$C_E=\frac{1}{\rho_e U_e}\frac{\mathrm{d}}{\mathrm{d}S}\int_0^\delta\rho U\mathrm{d}N \tag{15}$$

Here S and N are the streamwise and normal directions, respectively, within the boundary layer. The subscript e refers to the boundary-layer edge denoted by $N=\delta$. Within the confines of small disturbance theory the edge conditions may be taken as those corresponding to the inviscid solution along the wing surface or wake centerline evaluated on $\zeta=0^{\pm}$.

The primary dependent variables are taken as (θ/c_s), $\bar{H}$, and C_E. Given their value at any streamwise station ξ, their distributions may be predicted by the following system of first-order ordinary differential equations.

$$\frac{\mathrm{d}}{\mathrm{d}\xi}\left(\frac{\theta}{c_s}\right)=\frac{C_f\cos\Lambda_s}{2}-[H_0+2-M_e^2\cos^2\Lambda_s]\left(\frac{\theta}{c_s}\right)\left(\frac{1}{c}\right)\phi_{\xi\xi} \tag{16}$$

$$\frac{\mathrm{d}\bar{H}}{\mathrm{d}\xi}=\left(\frac{\theta}{c_s}\right)^{-1}\frac{\mathrm{d}\bar{H}}{\mathrm{d}H_1}\left\{C_E\cos\Lambda_s-H_1\left[\frac{C_f\cos\Lambda_s}{2}-(H_0+1)\left(\frac{\theta}{c_s}\right)\left(\frac{1}{c}\right)\phi_{\xi\xi}\right]\right\} \tag{17}$$

$$\frac{\mathrm{d}C_E}{\mathrm{d}\xi}=\left(\frac{\theta}{c_s}\right)^{-1}F_A\left\{\left(\frac{2.8}{H_0+H_1}\right)\cos\Lambda_s\left[(C_\tau)^{1/2}_{EQ_0}-\lambda_c(C_\tau)^{1/2}\right]+\left(\frac{\theta}{U_e}\frac{\mathrm{d}U_e}{\mathrm{d}S}\right)_{EQ}\cos\Lambda_s-\left[1+0.075M_e^2\cos^2\Lambda_s\left(\frac{1+0.2M_e^2\cos^2\Lambda_s}{1+0.1M_e^2\cos^2\Lambda_s}\right)\right]\left(\frac{\theta}{c_s}\right)\left(\frac{1}{c}\right)\phi_{\xi\xi}\right\} \tag{18}$$

A definition of the parameters necessary to complete the description of these equations may be found in Refs. 15-17.

In addition, it may be shown that

$$(\delta^*/c_s)_\xi=F_1+F_2\phi_{\xi\xi} \tag{19}$$

where

$$F_1=\left\{\frac{H_0C_f}{2}+\left[1+\left(\frac{\gamma-1}{2}\right)rM_e^2\right]\left(C_E-\frac{H_1C_f}{2}\right)\frac{\mathrm{d}\bar{H}}{\mathrm{d}H_1}\right\}\cos\Lambda_s \tag{20}$$

and

$$F_2=\left\{\left[1+\left(\frac{\gamma-1}{2}\right)rM_e^2\right](H_0+1)\frac{\mathrm{d}\bar{H}}{\mathrm{d}H_1}+(\gamma-1)rM_e^2\times\left[1+\left(\frac{\gamma-1}{2}\right)rM_e^2\right](\bar{H}+1)-H_0(H_0+2-M_e^2)\right\}\left(\frac{\theta}{c_s}\right)\left(\frac{1}{c}\right) \tag{21}$$

This form was first deduced by East et al.[17] and displays the dominant explicit dependence of the displacement surface slope upon the pressure gradient $\phi_{\xi\xi}$.

Modified Boundary Conditions

The effect of the viscous flow regions is accounted for in the inviscid solution by modifying the surface boundary condition to incorporate viscous displacement. Thus, Eq. (6) is replaced by

$$\phi_\zeta^\pm = (1/c) f_\xi^\pm + \epsilon k f_t^\pm + f_{R_\xi}^\pm \tag{22}$$

where the viscous ramp is used, and

$$\phi_\zeta^\pm = (1/c) f_\xi^\pm + \epsilon k f_t^\pm + (\delta^*/c_s)_\xi^\pm$$
$$= (1/c) f_\xi^\pm + \epsilon k f_t^\pm + (F_1 + F_2 \phi_{\xi\xi})^\pm \tag{23}$$

on $\zeta = 0^\pm$ for $0 \le \xi \le 1$, $0 \le \eta < \eta_{\text{tip}}$ when coupled with the lag entrainment equations. Downstream of the wing trailing edge the viscous wake generates an effective displacement afterbody. Due to its presence, a discontinuity in the slope of the potential is now permitted such that the wake condition Eq. (7b) is replaced by

$$[\phi_\zeta] = [(\delta^*/c_s)_\xi] = [F_1 + F_2 \phi_{\xi\xi}] \tag{24}$$

on $\zeta = 0$ for $\xi > 1$, $0 \le \eta \le \eta_{\text{tip}}$.

IV. Numerical Method

Inviscid Algorithm

The time accurate solution of the inviscid potential equation [Eq. (3)] is obtained by the following first-order (in time) accurate approximate factorization alternating direction implicit (ADI) algorithm.

ξ sweep:

$$B\overleftarrow{\delta}_\xi \left(\frac{\tilde{\phi} - \phi^n}{\Delta t} \right) = D_\xi \left[a^n \left(\frac{\tilde{\phi}_\xi + \phi_\xi^n}{2} \right) + b \phi_\xi^n \tilde{\phi}_\xi \right]$$
$$+ 2G_S (\delta_\eta \phi^n) D_\eta (\overleftarrow{\delta}_\xi \phi^n) + \delta_\eta (c \delta_\eta \phi^n) + c \delta_{\zeta\zeta} \phi^n + \delta_\xi X^n + \delta_\eta Y^n \tag{25a}$$

η sweep:

$$B\overleftarrow{\delta}_\xi \left(\frac{\tilde{\tilde{\phi}} - \tilde{\phi}}{\Delta t} \right) = \tfrac{1}{2} \delta_\eta (c \delta_\eta \tilde{\tilde{\phi}} - c \delta_\eta \phi^n) + G_S (\delta_\eta \phi^n) D_\eta (\overleftarrow{\delta}_\xi \tilde{\tilde{\phi}} - \overleftarrow{\delta}_\xi \phi^n) \tag{25b}$$

ζ sweep:

$$cA \left(\frac{\phi^{n+1} - 2\phi^n + \phi^{n-1}}{\Delta t^2} \right) + B\overleftarrow{\delta}_\xi \left(\frac{\phi^{n+1} - \tilde{\tilde{\phi}}}{\Delta t} \right) = \frac{c}{2} \delta_{\zeta\zeta} (\phi^{n+1} - \phi^n) \tag{25c}$$

Here, δ_ξ, δ_η, and $\delta_{\zeta\zeta}$ are second-order accurate central difference operators, $\overleftarrow{\delta}_\xi$ a first-order accurate backward difference operator, and D_ξ and D_η type-dependent mixed difference operators. Details of the numerical method are summarized in Ref. 10 and discussed in detail in Ref. 25.

Viscous Equations

The viscous ramp slope modification at time level $n+1$ ($f_{R_\xi}^{n+1}$) is evaluated based upon the potential distribution at time level n(ϕ^n). In order to locate the sonic point ξ_s, the simple sweep relationship

$$C_{p_{2D}} = C_{p_{3D}} / \cos^2 \Lambda_s \tag{26}$$

is employed, where the steady form of $C_{p_{3D}}$ is taken as is consistent with the quasisteady assumption. The sonic point is then defined such that

$$C_{p_{2D}} = C_{p_{2D}}^* \quad \text{at} \quad \xi = \xi_s \tag{27}$$

The critical pressure coefficient $C_{p_{2D}}^*$ is that corresponding to the equivalent two-dimensional freestream Mach number

$$M_{\infty_{2D}} = M_{\infty_{3D}} \cos \Lambda_s \tag{28}$$

The upstream location at which $\phi_{\xi_{US}}$ is evaluated corresponds to that grid point lying two mesh points upstream of ξ_s. Once ξ_s and $\phi_{\xi_{US}}$ are obtained, the entire ramp geometry is defined.

Solutions to the lag entrainment equations in the form given by Eqs. (16-18) are obtained by a simple second-order accurate Runge-Kutta integration scheme. Initial conditions are established upstream of shock waves for sections where the flow is locally supersonic or at the point of minimum pressure for sections where shock waves are absent. For this purpose incompressible flat plate results and a 1/7 power law velocity profile[26] are used to initialize θ, $\bar{H}$, and C_E. Integration is then carried out to the downstream boundary based upon the potential distribution at the previous time step.

Coupling Procedure

Far upstream of shock waves all viscous effects upon the inviscid solution are neglected. For locally supersonic stations the viscous ramp is employed ahead of the sonic location as a simple wing surface slope modification given by Eq. (22), but no coupling with the boundary-layer solution is invoked. Downstream of the sonic location the remaining portion of the viscous ramp is ignored and the boundary-layer solution is coupled implicitly to the inviscid solution through use of Eqs. (23) and (24). In the case of locally subsonic stations no viscous ramp is employed and the implicit coupling procedure is initiated at the point of minimum pressure.

The wing plane ($\zeta = 0$) is centered between planes of computational mesh points, such that the surface boundary condition is manifested in the calculation of $\phi_{\zeta\zeta}$ in the mesh planes just above and below $\zeta = 0$. This is accomplished by employing the relationship

$$(\phi_{\zeta\zeta})_{IJK_p} = (1/\Delta\zeta)^2 [(\phi_{IJK_p+1} - \phi_{IJK_p}) - \Delta\zeta (\phi_\zeta^+)_{IJ}] \tag{29}$$

where the index K_p refers to the mesh plane just above the wing surface and a constant mesh size is considered here for illustrative purposes. The surface boundary condition is now employed as

$$(\phi_\zeta^+)_{IJ} = (1/c_J)(f_\xi^+)_{IJ} + \epsilon k (f_t^+)_{IJ} + (F_1^+ + F_2^+ \phi_{\xi\xi}^+)_{IJ} \tag{30}$$

and $(\phi_{\xi\xi}^+)_{IJ}$ is written in terms of the potential at points lying above the surface; i.e.,

$$(\phi_{\xi\xi}^+)_{IJ} = (1/\Delta\zeta) [\zeta_{K_p+1} (\phi_{\xi\xi})_{IJK_p} - \zeta_{K_p} (\phi_{\xi\xi})_{IJK_p+1}] \tag{31}$$

Equations (30) and (31) are then used in conjunction with Eq. (29) to obtain

$$(\phi_{\zeta\zeta})_{IJK_p}^{n+1} = (1/\Delta\zeta)^2 \{ (\phi_{IJK_p+1}^{n+1} - \phi_{IJK_p}^{n+1})$$
$$- \Delta\zeta [(1/c_J)(f_\xi^+)_{IJ}^{n+1} + \epsilon k (f_t^+)_{IJ}^{n+1} + (F_1^+)_{IJ}^n]$$
$$- (1/\Delta\xi)^2 (F_2^+)_{IJ}^n [\zeta_{K_p+1} (\phi_{I+1JK_p}^n - 2\phi_{IJK_p}^{n+1} + \phi_{I-1JK_p}^{n+1})$$
$$- \zeta_{K_p} (\phi_{I+1JK_p+1}^n - 2\phi_{IJK_p+1}^{n+1} + \phi_{I-1JK_p+1}^{n+1})] \} \tag{32}$$

This expression forms an implicit relationship as part of the tridiagonal system in the ζ sweep of the inviscid algorithm. An

expression similar to Eq. (32) may be derived for $(\phi_{\xi\zeta})^{n+1}_{IJK_m}$. It is noted that at the grid location I,J values of ϕ at the upstream column $(\phi^{n+1}_{I-1,J})$ are known at the advanced time level but those at the downstream column $(\phi^{n}_{I+1,J})$ must be taken at the previous time level for the algorithm to remain intact. A similar treatment of the trailing wake may be formulated by use of Eq. (24). The coupling procedure is considered to be significant in suppressing numerical instabilities which would otherwise occur, particularly in regions where $(\delta^*/c_s)_\xi$ is large such as at the trailing edge.

V. Results

All of the results presented here were generated on a nonuniform $60\times40\times20$ (ξ,η,ζ) Cartesian computational mesh with the wing surface defined by 39×12 of these points in the ξ-η plane. The computational domain was defined by $-15.375\le\xi\le26.575$; $0\le\eta\le5.3$; $-13.0375\le\zeta\le13.0375$ and minimum grid spacing taken as

$$\Delta\xi_{\min}=0.01 \qquad \Delta\eta_{\min}=0.10 \qquad \Delta\zeta_{\min}=0.025$$

which occur at the wing leading edge, at the wing tip, and adjacent to the wing surface, respectively. A time step of $\Delta t=0.0043633$ was employed. This corresponds to a distance of one root chord of travel in 45.8 time steps at the freestream velocity. For a reduced frequency of $k=0.2$, the choice of Δt results in four time steps per degree of circular frequency change along the pitching cycle of a forced oscillation. Nominal values of the viscous ramp parameters were selected as follows.

$$\xi_o=0.02, \qquad \xi_p=0.02, \qquad \xi_R=0.10$$

These choices have proven adequate for a number of both steady and unsteady two-dimensional solutions.[14,20] Results were generated on the CDC 7600 computing system and required approximately 4 s of CPU time per time step of calculation for both inviscid and viscous cases.

In order to establish validity of the assumptions underlying the computational method, comparison is made with experimental data for the steady flow about a high aspect ratio wing having an advanced airfoil section. The configuration to be considered corresponds to the Lockheed-Georgia "wing A"[27,28] which was developed as part of a comprehensive program to acquire steady transonic experimental data specifically for evaluation of three-dimensional computational methods. The wing has an aspect ratio of 8.0, a taper ratio of 0.4, and leading edge sweep angle of 27 deg ($\eta_{\text{tip}}=2.77$). A nonuniform 12% thick airfoil section having appreciable aft camber is employed, with approximately 5 deg of nose-down twist occurring between the root and tip sections. The section and planform geometry are regarded as representative of modern transport aircraft.

Freestream conditions were established for the flow in air at $M_\infty=0.819$, $\alpha=1.96$ deg, and $Re_\infty=8.08\times10^6$. These values duplicate the test conditions of Hinson and Burdges[27,28] as well as the numerical results of Streett.[29] A steady-state solution was generated by the time integration procedure previously summarized, with initial conditions corresponding to an undisturbed flow ($\phi=\phi_t=0$). Results of this calculation are shown in Fig. 2 in terms of the wing surface pressure distribution where the data of Hinson and Burdges have been provided for comparison. The spanwise mesh distribution was selected to coincide with experimental data measuring stations. Figure 2 shows good agreement between the computed pressure distribution and the experimental data at all span stations for which measurements are available.

A more detailed presentation of these results is provided in Fig. 3 which shows the chordwise surface pressure distribution at the 70% span station. In addition, a fully inviscid solution for this same case was computed and shown

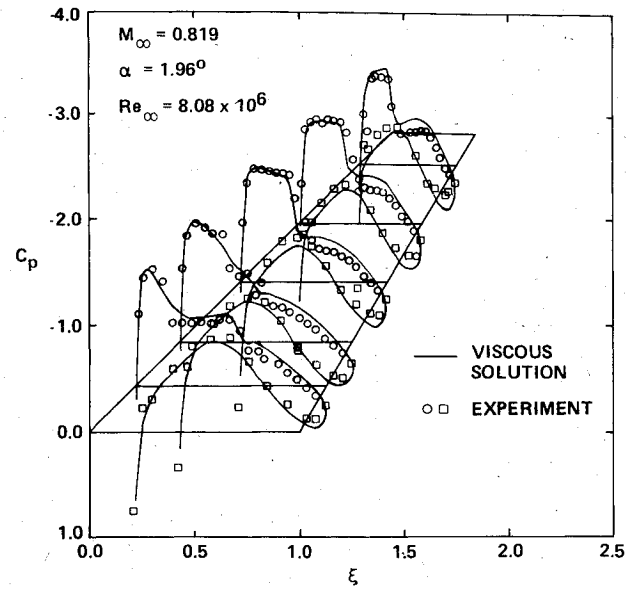

Fig. 2 Comparison of steady surface pressure distributions with experiment for Lockheed "wing A."

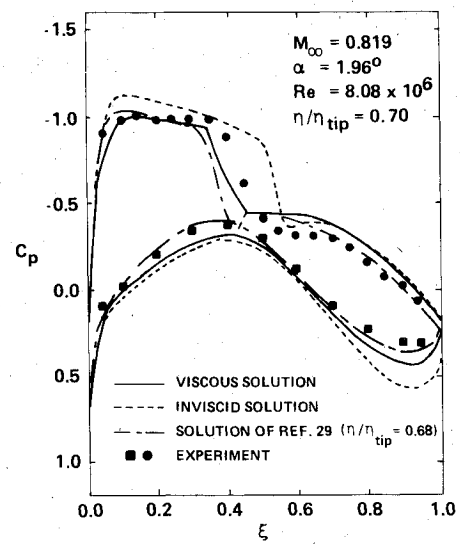

Fig. 3 Comparison of steady surface pressure distribution with experiment for Lockheed "wing A" at $\eta/\eta_{\text{tip}}=0.70$.

for comparison. The improvement due to the addition of the boundary-layer calculation is apparent. It is noted that the shock is weakened and displaced upstream by the inclusion of viscous effects. Aft decambering due to the boundary-layer displacement is quite noticeable, particularly on the lower surface. Also shown are the numerical results of Streett[29] which consist of a full potential inviscid outer flow solution and a fully three-dimensional integral boundary-layer and wake solution coupled via the displacement thickness. While the flow conditions for Streett's solution are the same as previously noted, the configuration consists of a half-body fuselage model with a midmounted wing and corresponds to another of the test cases of Hinson and Burdges. Streett's result compared extremely well with experiment, thus the data for the wing-body combination has been omitted. Due to the presence of the body, the shock lies somewhat ahead of its location for the wing alone. The lower surface pressure distribution is virtually the same in both cases.

Upper surface distributions of the displacement and momentum defect thickness at midspan appear in Fig. 4. Influence of the shock can be seen near $\xi=0.4$. Downstream

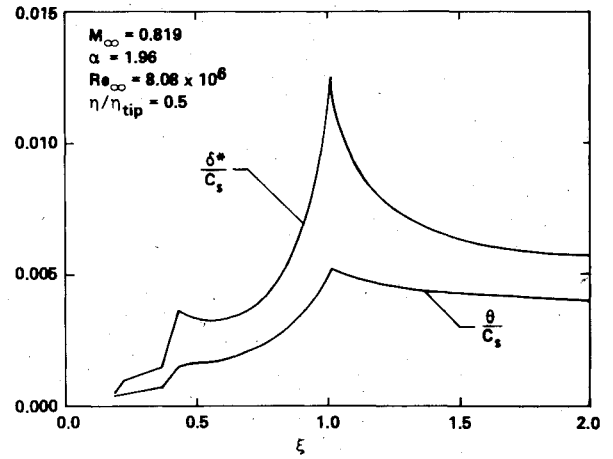

Fig. 4 Steady upper surface displacement and momentum defect thickness distributions for Lockheed "wing A."

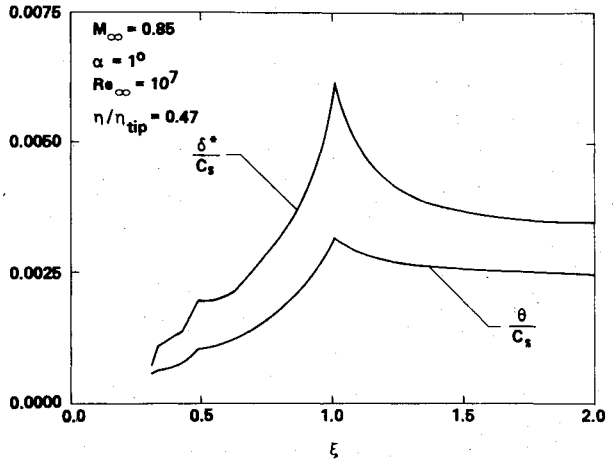

Fig. 6 Steady upper surface displacement and momentum defect thickness distributions for MBB-A3 wing.

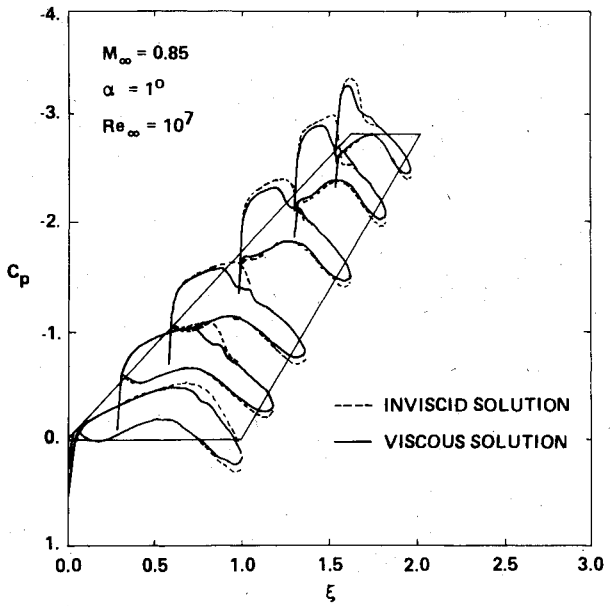

Fig. 5 Comparison of inviscid and viscous steady surface pressure distributions for MBB-A3 wing.

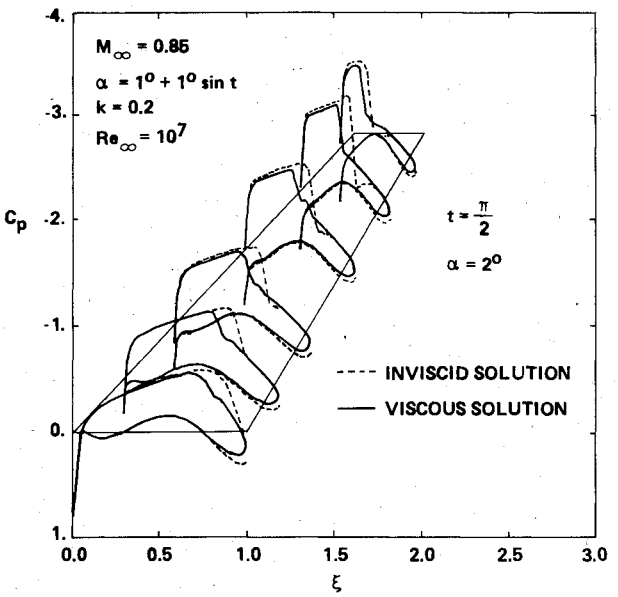

Fig. 7a Comparison of inviscid and viscous unsteady surface pressure distributions for MBB-A3 wing at $t = \pi/2$ and $\alpha = 2$ deg.

of the trailing edge, θ and δ^* tend to constant values which is consistent for wakes without pressure gradient.

In the case of fully three-dimensional unsteady transonic flows over wings, little experimental data suitable for validation purposes is available. Because of this, a representative sample calculation was selected in order to illustrate results of the numerical method. For this example a section geometry corresponding to the MBB-A3[30] airfoil was chosen. The section has a blunt leading edge, a thickness ratio of 8.9%, moderate aft camber, and has been selected as an AGARD standard for evaluating transonic aeroelastic analysis methods. A wing planform identical to the Lockheed-Georgia "wing A" was employed ($AR = 8.0$, $\lambda = 0.4$) except that the leading edge sweep angle was set to 30 deg.

Steady-state viscous and inviscid solutions were generated for freestream conditions corresponding to $M_\infty = 0.85$, $\alpha = 1.0$ deg, and $Re_\infty = 10^7$. Results of the pressure distributions at half of the spanwise mesh stations are compared in Fig. 5. Viscous effects near shocks and on the aft lower surface are apparent. Corresponding chordwise distributions of the displacement and momentum defect thickness near the midspan station appear in Fig. 6.

Using the steady-state solutions as initial conditions, an unsteady calculation was performed by specifying a forced

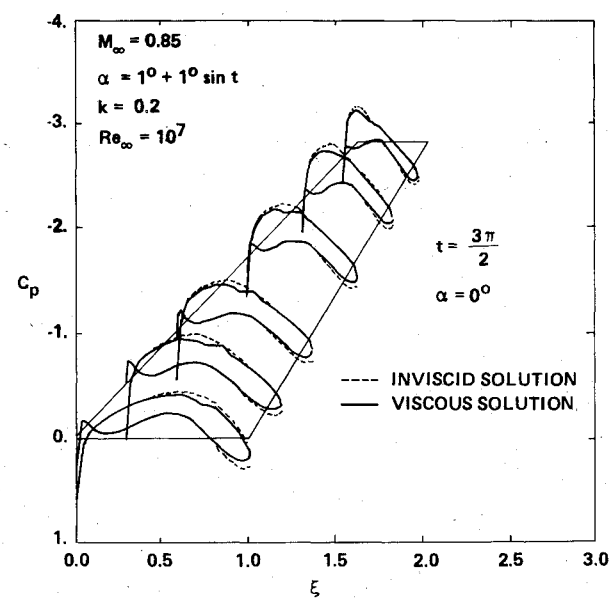

Fig. 7b Comparison of inviscid and viscous unsteady surface pressure distributions for MBB-A3 wing at $t = 3\pi/2$ and $\alpha = 0$ deg.

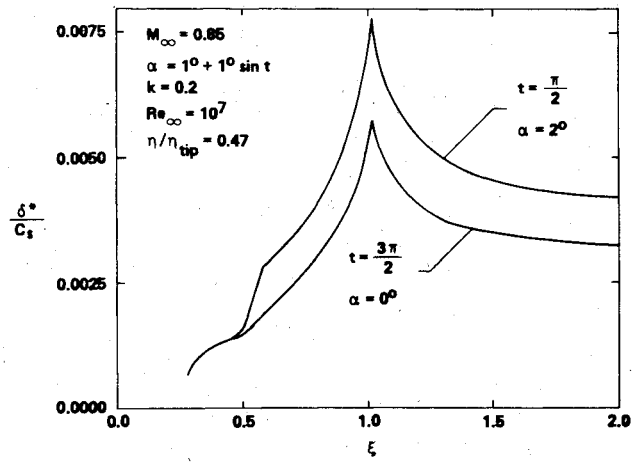

Fig. 8 Unsteady upper surface displacement thickness distribution for MBB-A3 wing.

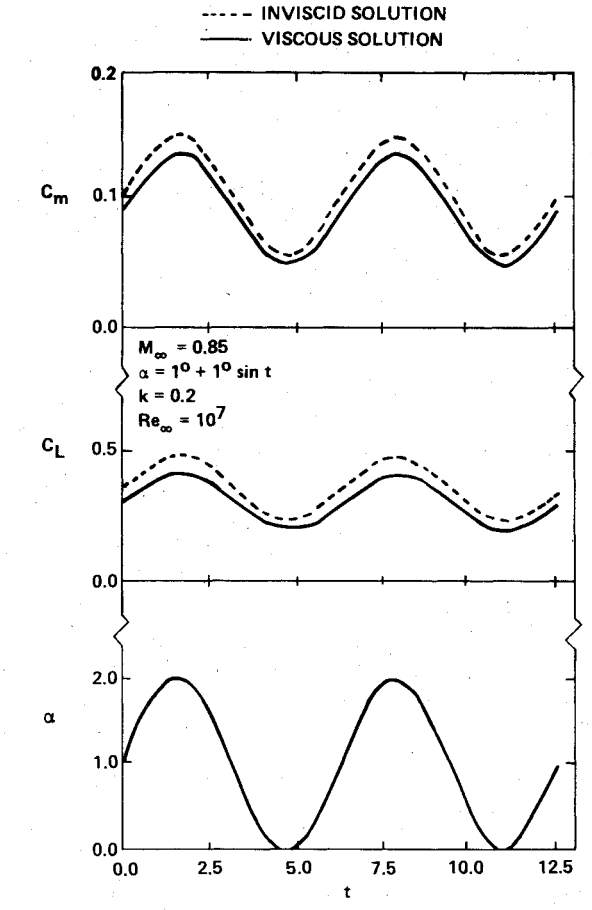

Fig. 9 Unsteady lift and moment coefficients for MBB-A3 wing.

rotation about the wing leading edge root such that $\alpha = 1$ deg + 1 deg sin$t$. The reduced frequency, k, was chosen to be 0.2, and for simplicity the low-frequency approximation was made ($\epsilon = 0$). Integration in time was allowed to proceed for two cycles of rotation. Figure 7 indicates the instantaneous surface pressure distribution for this case. The value of time here is referenced to the beginning of the second cycle and given in radians. At the maximum angle of attack, $\alpha = 2$ deg (Fig. 7a), a large difference between the solutions, particularly near shocks is evident. While the difference between the solutions is less substantial at the minimum angle of attack, $\alpha = 0$ deg (Fig. 7b), aft decambering due to viscous displacement is still appreciable. Corresponding values of the displacement thickness are given in Fig. 8. It is noted that the large differences in δ^* at the extremes of the oscillation cycle are brought about by the alternate formation and disappearance of the shock. In Fig. 9 the total wing unsteady lift and moment coefficient time histories are presented along with the angle-of-attack variation. Although there is little phase difference between the inviscid and viscous solution for this particular case, the difference in both mean value and magnitude of oscillation is significant.

VI. Discussion and Conclusions

A method has been presented for computing the unsteady three-dimensional transonic flowfield about thin wings of arbitrary planform and section geometry including the effects of inviscid/viscous interaction. Dominant effects of the shock/boundary-layer interaction were accounted for by a simple computational artifice, while viscous regions adjacent to the wing surface and along the trailing wake were described by a set of integral equations appropriate for two-dimensional turbulent flows. Although this analysis necessarily was simplified, comparison with steady three-dimensional experimental data and a solution of more exact equations for a typical transport configuration indicates that it will be adequate for many practical applications. In addition, an example calculation of a wing oscillating in rotation indicated appreciable variation in unsteady aerodynamic force coefficients when viscous effects are accounted for. This behavior is typical of wings having advanced airfoil sections and may be a significant consideration when performing aeroelastic analysis.

No provision has been made in the present work for the existence of a laminar portion of the upstream boundary layer. For the results considered here, the Reynolds numbers were sufficiently large such that for practical purposes the entire boundary layer could be considered turbulent. A simple attachment line model or stagnation point solution followed by a laminar calculation and suitable transition criteria could be incorporated easily in order to establish initial conditions for the lag entrainment equations without altering the basic computational method. Wake curvature effects have been neglected entirely in the results presented here. These may be accounted for by a simple alteration of the basic wake jump condition, Eq. (7a).[29] It is indicated by the results of Streett[29] that wake curvature may have a significant impact upon the lower surface pressure distribution for wings having advanced airfoil sections. It should also be noted that the method is designed to compute attached flows only, although in practice the numerical procedure may tolerate small regions of separation.

The method of time integration of fluid dynamic equations of motion offers a unique capability for performing aeroelastic analysis. Unsteady structural equations of motion governing the deformation of an elastic wing may be coupled with these directly and simultaneously integrated in time to determine the aeroelastic response of the combined system. This technique has already been applied for a purely inviscid flowfield,[13] and may be extended easily to include viscous effects by the described method. Addition of the integral equations for viscous calculations increases computation time (CPU) by less than 6%, thus maintaining the basic efficiency of the inviscid algorithm. This consideration provided much of the motivation for employing a simplified viscous analysis, and appears to be justified for the purpose of structural applications.

Acknowledgments

The work reported here was sponsored in part by NASA under Contract NAS2-10762. Computation time on the CDC 7600 at NASA/Ames Research Center was provided through auspices of the Applied Computational Aerodynamics Branch.

References

[1] Ballhaus, W. F. and Bailey, F. R., "Numerical Calculation of Transonic Flow About Swept Wings," AIAA Paper 72-677, June 1972.

[2] Lomax, H., Bailey, F. R., and Ballhaus, W. F., "On the Numerical Simulation of Three-Dimensional Transonic Flow with Application to the C-141 Wing," NASA TN D-6933, Aug. 1973.

[3] Boppe, C. W., "Calculation of Transonic Wing Flows by Grid Embedding," AIAA Paper 77-207, Jan. 1977.

[4] Mason, W., Mackenzie, D. A., Stern, M. A., and Johnson, J. D., "A Numerical Three-Dimensional Viscous Transonic Wing-Body Analysis and Design Tool," AIAA Paper 78-120, Jan. 1978.

[5] Jameson, A. and Caughey, D. A., "A Finite Volume Method for Transonic Potential Flow Calculations," AIAA Paper 77-635, June 1977.

[6] Holst, T. L., "A Fast, Conservative Algorithm for Solving the Full-Potential Equation," AIAA Paper 79-1456, July 1979.

[7] Boppe, C. W. and Stern, M. A., "Simulated Transonic Flows for Aircraft with Nacelles, Pylons, and Winglets," AIAA Paper 80-104, Jan. 1980.

[8] Caradonna, F. X. and Isom, M. P., "Numerical Calculation of Unsteady Transonic Potential Flow Over Helicopter Rotor Blades," *AIAA Journal,* Vol. 14, April 1976, pp. 482-488.

[9] Caradonna, F. X. and Phillippe, J. J., "The Flow Over a Helicopter Blade Tip in the Transonic Regime," *Vertica,* Vol. 2, No. 1, 1978, pp. 43-60.

[10] Borland, C., Rizzetta, D., and Yoshihara, H., "Numerical Solution of Three-Dimensional Unsteady Transonic Flow over Swept Wings," AIAA Paper 80-1369, July 1980.

[11] Steger, J. L. and Caradonna, F. X., "A Conservative Implicit Finite Difference Algorithm for the Unsteady Transonic Full Potential Equation," AIAA Paper 80-1368, July 1980.

[12] Sankar, N. L., Malone, J. B., and Tassa, Y., "An Implicit Conservative Algorithm for Steady and Unsteady Three-Dimensional Transonic Potential Flows," AIAA Paper 81-1016, June 1981.

[13] Borland, C. J. and Rizzetta, D. P., "Nonlinear Transonic Flutter Analysis," *AIAA Journal,* Vol. 20, Nov. 1982, pp. 1606-1615.

[14] Rizzeta, D.P. and Yoshihara, H., "Computations of the Pitching Oscillation of a NACA 64A-010 Airfoil in the Small Disturbance Limit," AIAA Paper 80-0128, Jan. 1980.

[15] Green, J. E., "Application of Head's Entrainment Method to the Prediction of Turbulent Boundary Layers and Wakes in Compressible Flow," RAE Reports and Memoranda 3788, April 1972.

[16] Green, J. E., Weeks, D. J., and Brooman, J. W. F., "Prediction of Turbulent Boundary Layers and Wakes in Compressible Flow by a Lag-Entrainment Method," RAE Reports and Memoranda 3791, Jan. 1973.

[17] East, L. F., Smith, P. D., and Merryman, P. J., "Prediction of the Development of Separated Turbulent Boundary Layers by the Lag-Entrainment Method," RAE Tech. Rept. 77046, March 1977.

[18] Wai, J. C. and Yoshihara, H., "Viscous Transonic Flow Over Airfoils," *Proceedings of the Seventh International Conference on Numerical Methods in Fluid Dynamics,* Palo Alto, Calif., June 1980, pp. 417-422.

[19] Wai, J. C. and Yoshihara, H., "Planar Transonic Airfoil Computations with Viscous Interactions," AGARD-CP-291, Sept. 1980, pp. 9-1 - 9-9.

[20] Rizzetta, D. P., "Procedures for the Computation of Unsteady Transonic Flows Including Viscous Effects," NASA CR-166249, Aug. 1981.

[21] Mason, W. H., Ballhaus, W. F., Mackenzie, C., Frick, J., and Stern, M., "An Automated Procedure for Computing the Three-Dimensional Transonic Flow over Wing-Body Combinations, Including Viscous Effects," AFFDL-TR-77-122, Vol. I, Feb. 1977.

[22] Rizzetta, D. P. and Yoshihara, H., "Oscillating Supercritcal Airfoils in the Transonic Regime with Viscous Interactions," AGARD-CP-296, Sept. 1980, pp. 2-1 - 2-7.

[23] Bradshaw, P., Ferriss, D. H., and Atwell, N. P., "Calculation of Turbulent Boundary-Layer Development Using the Turbulent Energy Equations," *Journal of Fluid Mechanics,* Vol. 28, Part 3, May 1967, pp. 593-616.

[24] Head, M. R., "Entrainment in the Turbulent Boundary Layer," ARC Reports and Memoranda 3152, 1958.

[25] Borland, C. J. and Rizzetta, D. P., "Transonic Unsteady Aerodynamics for Aeroelastic Applications—Vol. I: Technical Development Summary," AFWAL TR-80-3107, Vol. I, May 1981.

[26] Schlichting, H., *Boundary Layer Theory,* McGraw-Hill, New York, N.Y., 1960, pp. 536-537.

[27] Hinson, B. L. and Burdges, K. P., "Acquisition and Application of Transonic Wing and Far-Field Test Data for Three-Dimensional Computational Method Evaluation—Volume I," AFSOR-TR-80-0421, March 1980.

[28] Hinson, B. L. and Burdges, K. P., "Acquisition for Application of Transonic Wing and Far-Field Test Data for Three-Dimensional Computational Method Evaluation—Volume II," AFSOR-TR-80-0422, March 1980.

[29] Streett, C. L., "Viscous-Inviscid Interaction for Transonic Wing-Body Configurations Including Wake Effects," AIAA Paper 81-1266, June 1981.

[30] Bland, S. R., "AGARD Two-Dimensional Aeroelastic Configurations," AGARD-AR-156, Aug. 1979.